Journal of Molecular Catalysis A: Chemical 350 (2011) 35–39

Contents lists available at SciVerse ScienceDirect

Journal of Molecular Catalysis A: Chemical

journal homepage: www.elsevier.com/locate/molcata

# Study of synthesis and catalytic property of $WO_3/TiO_2$ catalysts for NO reduction at high temperatures

He Zhang[a], Jian Han[a], Xiaowei Niu[a], Xu Han[a], Guodong Wei[a,b,*], Wei Han[a,**]

[a] Physical College, Jilin University, Qianjin Street 2699, Changchun City, Jilin Province 130012, PR China
[b] College of Science, Ningbo University of Technology, Cuibai Road, Ningbo City, Zhejiang Province 315016, PR China

ARTICLE INFO

*Article history:*
Received 23 June 2011
Received in revised form 3 September 2011
Accepted 3 September 2011
Available online 16 September 2011

*Keywords:*
SCR
High temperature
NO
$WO_3/TiO_2$
Sol–gel

ABSTRACT

In this study, a series of $WO_3$-*m*%/$TiO_2$ samples were successfully prepared via a simple and effective sol–gel method, which were subsequently used for the NO reduction by $NH_3$ in the temperature range of 350–600 °C. Structural, morphological, and BET analysis revealed that the $WO_3$ species were dispersed evenly into titania matrix so that the samples only exhibited anatase phase with high surface area. SCR results proved that the $WO_3/TiO_2$ catalysts exhibited good catalytic properties for the NO reduction at high temperatures. The correlated relationship between compositions, temperatures and structures for $WO_3/TiO_2$ catalytic mechanism was also discussed.



## 1. Introduction

The selective catalytic reduction (SCR) with ammonia has been considered as one of the most attractive techniques for the removal of nitrogen oxides ($NO_x$) from exhaust gas due to its efficiency, selectivity and economy [1–4]. $V_2O_5$–$WO_3$(Mo)/$TiO_2$, as one of the most promising industrial SCR catalyst, has been widely applied in this field due to its high activity and stability with a narrow temperature window of 300–400 °C [4,5].

However, although some progress has been made in this field, these vanadium-base catalysts still have some disadvantages. Besides its toxicity nature, the vanadium as the active component can also induce the oxidation of $SO_2$ to $SO_3$ in the exhaust gas, which can further react with $H_2O$ and slipped $NH_3$ to form ammonium bisulfate ($NH_4HSO_4$). Unfortunately, this formed solid salt can cover the catalyst surface and result in the catalyst failure. In addition, the enhanced sulfur poisoning resulted from the generated $SO_3$ can shorten the life of the catalysts with the increase of unreacted ammonia amount. More importantly, when the temperature is raised above 500 °C, $V_2O_5$-based catalysts can lose their SCR activity due to the direct oxidation reaction of ammonia with oxygen [6]. Therefore, considering the above emerged problems, many researchers have being attempted to develop novel environmentally friendly $NH_3$-SCR catalysts to instead the vanadium by other metal oxides. Xu et al. [7] developed a promising $NH_3$-SCR catalyst, $CeO_2/TiO_2$, which has been proved to have high activity in the temperature range of 275–400 °C. Subsequently, Chen et al. successfully enhanced its catalytic activity via doping vanadium [8] and tungsten [9] in the $CeO_2/TiO_2$ catalyst. Furthermore, the modification of tungsten on the surface properties of catalysts and the relevant $NH_3$-SCR reaction mechanisms of $CeO_2(WO_3)/TiO_2$ were also explored particularly by Chen's group [10].

$WO_3/TiO_2$ could be regarded as a promising catalyst with a good SCR performance, especially at high temperatures (over 500 °C) [11], and this catalyst has already attracted more and more attentions on the morphological properties, the acidities, the structures of supported $WO_x$ species and catalytic behavior in the SCR reaction [12–14]. To date, $WO_3/TiO_2$ catalysts have been prepared by impregnation [11–13], co-precipitation [15], and sol–gel method [16]. At the same time, the effects of difference prepared methods on the SCR performance have been investigated [15]. Yang et al. [16] reported the synthesis of $WO_3/TiO_2$ samples via the sol–gel method to investigate their photocatalytic properties. However, the SCR catalytic behavior of $WO_3/TiO_2$ catalyst prepared by sol–gel method at remarkably higher temperatures (over 500 °C) has scarcely been reported.

In this present paper, in order to develop a promising SCR catalyst without vanadium and achieve its high temperature catalytic properties, $WO_3/TiO_2$ samples with different tungsten loadings

* Corresponding author at: Physical College, Jilin University, Qianjin Street 2699, Changchun City, Jilin Province 130012, PR China. Tel.: +86 0431 85167869; fax: +86 0431 85167869.
** Corresponding author. Tel.: +86 0431 85167869; fax: +86 0431 85167869.
*E-mail addresses:* wgd588@163.com (G. Wei), whan@jlu.edu.cn (W. Han).

1381-1169/$ – see front matter © 2011 Elsevier B.V. All rights reserved.
doi:10.1016/j.molcata.2011.09.001

have been successfully prepared by the sol–gel method. $NO_x$ conversions of these samples at high temperatures (ranging from 350 to 600 °C) were investigated. Moreover, the effects of different tungsten species on acidity, reducibility and SCR performance of $WO_3/TiO_2$ were also discussed particularly.

## 2. Experimental details

### 2.1. Catalysts preparation

All reagents used in this work were of analytical grade without any further purification. In a typical preparation process: Firstly, butyl titanate, anhydrous alcohol and acetic acid (with the molar ratio of 1:1:6) were ultrasonically dispersed to form a mixture solution. Then, different additions of ammonium tungstate solution were dripped into the above-prepared mixture according to the required amount of $WO_3$. Subsequently, the gained solution was stirred for 1 h, and then aged to obtain the gel. Finally, the $WO_3/TiO_2$ catalysts can be obtained after the gel was dried at 60 °C for 10 h in a drying oven and calcined at 600 °C for 5 h in the air. In addition, the samples contained *m* wt.%-$WO_3$ was denoted as W*m*/Ti hereafter.

### 2.2. Catalytic activity test

Catalytic measurements were carried out in a quartz tubular fixed bed continuous-flow reactor (inner diameter of 10 mm) containing catalysts of 400 mg. A feed gas mixture contained 500 ppm NO, 500 ppm $NH_3$, 5 vol.% $O_2$ and $N_2$ as the balance gas. In the test process, the total flow rate was fixed at 200 mL/min, which corresponded to a GHSV (gas hourly space velocity) of 30,000 $h^{-1}$. The flow can be accurately measured and controlled by means of mass flow meters and controllers. The gas compositions were monitored by infrared gas analyzer (QGS-08C) and flue gas analyser (KM9106). Activity data have been collected at different temperatures in the range of 350–600 °C with a size step increment of 50 °C for each settled temperature which was maintained until steady-state conditions were reached. The conversion of $NO_x$ [$X(NO_x)$] is defined by Eq. (1):

$$X(NO_x) = \frac{[NO_x]_{inlet} - [NO_x]_{outlet}}{[NO_x]_{inlet}} \times 100\% \quad (1)$$

with $[NO_x] = [NO] + [NO_2]$.

### 2.3. Characterization of catalysts

The structures of samples were examined using a powder X-ray diffractometer Japan D/max-RA instrument with Cu Kα radiation (λ = 1.5418 Å, tube voltage = 50 kV, tube current = 150 mA) from 10° to 90° with a scan step size of 0.02°. The characterization of BET surface area of the samples was determined by a Micromeritics ASAP 2020 apparatus. The morphology was observed by a transmission electron microscope (TEM, H8160, Japan). Raman spectra were performed on a J&Y-Raman-T64000 spectrometry with an Ar ion laser of 532 nm excitation wavelength at ambient conditions.

The reducibility of surface species for these samples was determined by temperature programmed reduction ($H_2$-TPR) experiment performed on a chemisorption analyzer (Micromeritics, ChemiSorb 2720 TPx) under a 10% hydrogen–90% nitrogen gas flow (50 mL/min) at a rate of 10 °C/min up to 950 °C.

Ammonia temperature programmed desorption ($NH_3$-TPD) experiments were performed in a quartz tubular fixed bed microreactor inserted into an electric furnace driven by a PID temperature controller/programmer. The outlet of the reactor was connected to a Gas Chromatograph (GC model 8A) for the continuous analysis of the gases exiting the reactor. The samples were pretreated in an Ar stream at 500 °C for 60 min. Ammonia was passed at 100 °C; the samples were then purged with Ar at 100 °C for 120 min and finally temperature was raised at 10 °C/min up to 500 °C in a nitrogen stream.

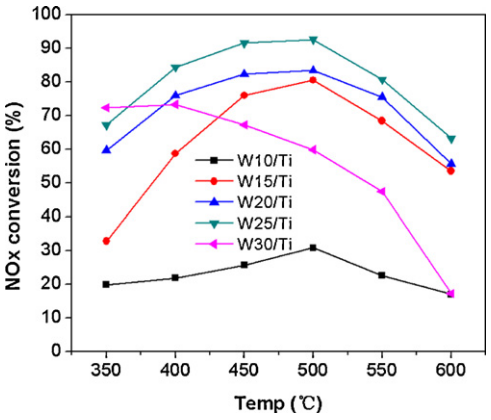


**Fig. 1.** $NO_x$ conversion of W*m*/Ti catalysts with different $WO_3$ loadings.

## 3. Results and discussion

### 3.1. Results of activity test

The catalytic activities dependence of $WO_3$ loading contents and temperatures were investigated by the activity tests. The experimental curves of the catalytic tests for $NO_x$ reduction by $NH_3$ performed over the W*m*/Ti samples are displayed in Fig. 1. From Fig. 1, the catalytic activities of samples increase with the $WO_3$ loading content from 10% to 25%, however, W30/Ti sample presented worse catalytic activities at the temperatures above 400 °C compared with W25/Ti. At the same time, for each W*m*/Ti sample except for W30/Ti, the catalytic curves display the same trend over temperature, namely, the $NO_x$ conversion is advanced with the growth of temperature from 350 to 500 °C and reduce gradually with growth of the temperature from 500 to 600 °C. Obviously, the W25/Ti sample shows the best catalytic performances with the $NO_x$ conversion beyond 80% in the temperature range of 400–550 °C and has the maximum value of 92% at 500 °C. Although the catalytic activities of W25/Ti begin to decline when the temperature is beyond 500 °C, the value of $NO_x$ conversion is even as high as 65% at 600 °C.

### 3.2. Results of characterization

#### 3.2.1. XRD and morphology

The crystalline structures of the samples were examined by XRD. As shown in Fig. 2, only anatase phase can be detected in these samples. It is noted that the crystalline $WO_3$ phase in the XRD pattern cannot be found, even when the $WO_3$ loading content is as high as 30%. Thus, it is suggested that the $WO_3$ species are present in either an amorphous state or small crystallites with less than 4 nm in diameter which are undetectable by XRD [15]. In addition, when $WO_3$ loading increasing to 15%, a very interesting phenomenon can be observed that two discrete peaks at 53.9° and 55° are integrated into one broad peak at 54.6°, which can be regarded as a rutile phase in the literature [17]. The similar phenomenon also takes place at around 70°. However, besides the peaks centered at 54.6° and 70°, there was no another characteristic peak of the rutile phase, and thus the syncretic peaks at 54.6° and 70° cannot be attributed to the rutile phase. This phenomenon may be due to the following reasons: (1) $W^{n+}$ ions entering into the $TiO_2$ crystalline lattice induce the $TiO_2$ crystalline lattice distortion [17] and

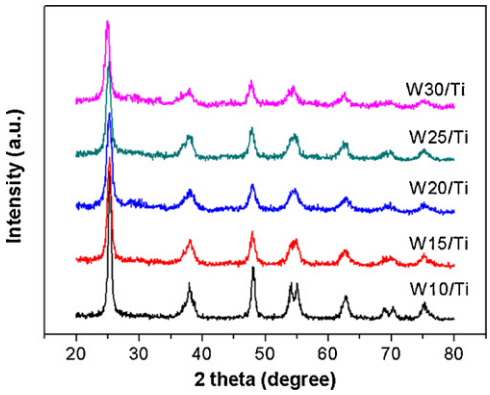


**Fig. 2.** XRD profiles of W*m*/Ti catalysts with different $WO_3$ loadings.

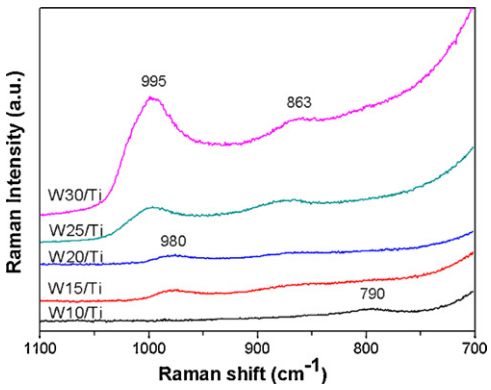


**Fig. 4.** Raman profiles of W*m*/Ti catalysts with different $WO_3$ loadings.

**Table 1**
Phase compositions, crystal sizes, and BET surface areas of the prepared catalysts. Dc, crystallite dimensions calculated by Scherrer Equation; Sa, BET surface area; Pv, pore volume; Dp, pore diameter.

| Samples | Phase | Dc (nm) | Sa ($m^2$/g) | Pv ($cm^3$/g) | Dp (nm) |
|---|---|---|---|---|---|
| W10/Ti | Anatase | 14.4 | 44.5 | 0.035 | 1.808 |
| W15/Ti | Anatase | 10.6 | 85.5 | 0.087 | 1.715 |
| W20/Ti | Anatase | 10.1 | 97.8 | 0.127 | 2.650 |
| W25/Ti | Anatase | 8.0 | 147.2 | 0.153 | 1.890 |
| W30/Ti | Anatase | 9.8 | 130.3 | 0.160 | 2.093 |

(2) more $WO_3$ additives lead to the diminishing of the crystal grains and the broadening of the double diffractive peaks.

BET surface area technology was used for disclosing the structure and surface properties of the samples. Table 1 presents the phase compositions, mean crystallite dimensions (Dc) (calculated from XRD measurements according to Scherrer Equation), surface areas (Sa), pore volumes (Pv) and mean pore diameters (Dp) for all catalysts. From Table 1, the average crystalline grain sizes calculated from XRD measurements decrease from 14 to 8 nm with the tungsten component increasing up to 25%. The surface areas of samples increase from 44.5 (W10/Ti) to 147.2 $m^2$/g (W25/Ti), however, when the $WO_3$ loading is beyond 25%, the BET value begins to slight decline. This behavior can be explained as follows [15]: more $WO_3$ additives used in the sol–gel preparation process can not only inhibit the crystal size growth of anatase, but also result in the increasing of the surface area at the same time. It is well known that, larger surface area can enhance the catalytic activity of the catalysts. In addition, when the $WO_3$ content is beyond 25 wt.%, the further increase of its content can result in the decreasing of samples surface area due to the larger density of $WO_3$ ($WO_3/TiO_2$ ratio in density is equal to ~1.7), which is unbeneficial for SCR catalytic application.

Fig. 3 presents typical TEM images of W25/Ti sample. As displayed in Fig. 3a, the particles with irregular shape are about several hundred nanometers in diameter. Obviously, these particles are not well discrete and aggregate to some extent, which can be assigned to the high calcination temperature of 600 °C and the high content loading of $WO_3$ which resulted in aggregation of the nanoparticles and porosity. Actually, as revealed in Fig. 3b, one single nanoparticle is composed of thousands of quite tiny particles with only several nanometers in diameter, which further supports the results obtained from the BET and XRD. The selected-area electron diffraction (SAED, inset of Fig. 3b) pattern of these nanoparticles demonstrates that the nanoparticles are not well crystallized and are polycrystalline in nature.

### 3.2.2. Raman

The Raman spectra of the samples are presented in Fig. 4. As displayed in Fig. 4, the weak band around 790 $cm^{-1}$ can be assigned to a second order feature of anatase titania [17] for W10/Ti sample and disappears when the $WO_3$ loading is over 15%. Additionally, characteristic Raman peaks of crystalline $WO_3$ at ~806 and 715 $cm^{-1}$ [13,18] were not detected even the $WO_3$ loading was up to 30 wt.%, which indicates that the tungsten species are highly dispersed into titania crystal lattice matrix.

According to the reported literatures [19–23], the Raman peak of tetrahedrally ($\nu_s$(W=O)) and octahedrally ($\nu$(W=O)) coordinated polymeric tungsten oxide species can be usually found in the range of 950–1050 $cm^{-1}$. Thus, it cannot be clearly determined which one

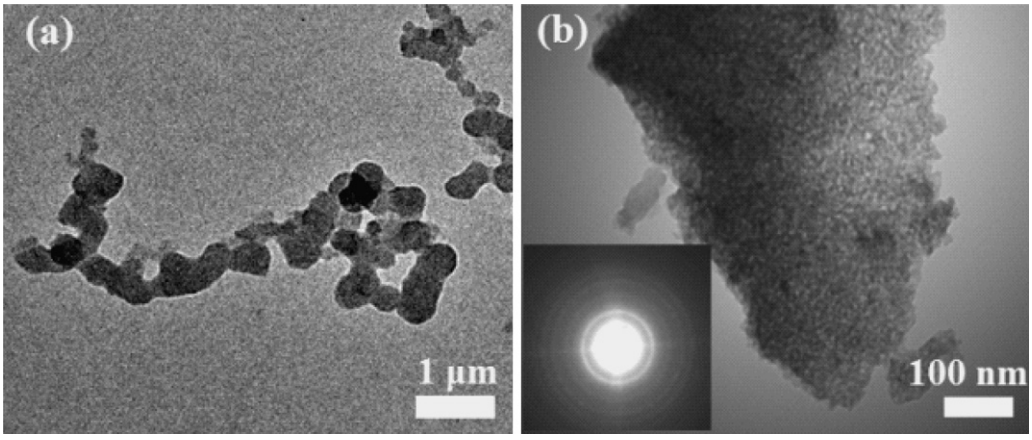


**Fig. 3.** TEM images of W25/Ti sample with different magnifications.

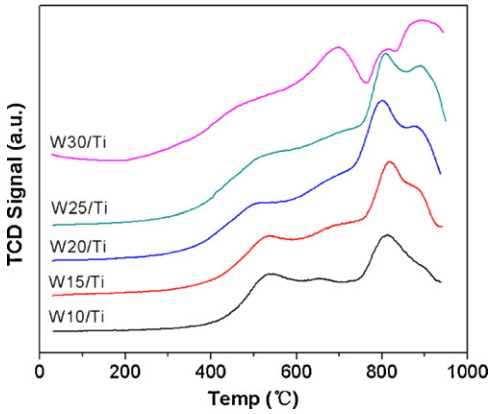


**Fig. 5.** $H_2$-TPR profiles of W*m*/Ti catalysts with different $WO_3$ loadings.

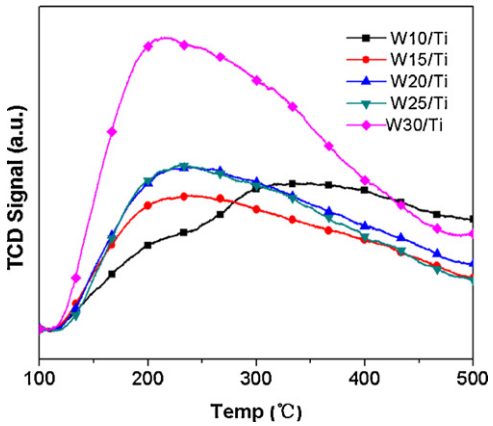


**Fig. 6.** $NH_3$-TPD profiles of W*m*/Ti catalysts with different $WO_3$ loadings.

tungsten oxide species according to Raman spectra due to their overlapped Raman bands in this district. The broad band approximately extending from 830 to 910 $cm^{-1}$ belongs to tetrahedrally coordinated $WO_x$ species ($\nu_{as}$(W=O)) [24]. Considering the literatures and our TPR results discussed later, we can assign the increase of the bands centered at 995 and 980 $cm^{-1}$ to the tetrahedrally coordinated species.

### 3.2.3. $H_2$-TPR

Fig. 5 shows the $H_2$-TPR profiles of the as-grown catalysts. The peaks ranged in 400–600 °C could be attributed to the octahedral coordinated $WO_x$ species, which can be usually reduced progressively in two stages: $W^{6+}$–$W^{5+}$–$W^{4+}$ [25,26]. The peaks appearing at higher temperatures (over 700 °C) could be attributed to the reduction of amorphous tetrahedral $WO_x$ species [20,26]. In addition, the peaks at around 810 and 900 °C present the similar trend with the increase of $WO_x$ component up to 25%. However, for W30/Ti, a big peak appears at about 705 °C, instead the increasing of the respective peaks at 810 and 900 °C. Horsley et al. [20] reported that at concentrations below the monolayer, tetrahedral $WO_x$ species are extremely difficult to be reduced because of a strong interaction between the isolate and dimeric state tungsten species and support. Their reducibility becomes easier at higher loading [25,27]. In addition, there are no other new phases detected by XRD and Raman in our catalysts. Therefore, the peak at 705 °C could be assigned to aggregation tetrahedral $WO_x$ species.

The $H_2$-TPR spectra demonstrate that tetrahedral $WO_x$ gradually increase with the $WO_x$ component loading up to 25%, but tetrahedral $WO_x$ begins to agglomerate when the loading is increasing from 25% to 30%. Therefore, based on the analysis of Raman, activity test and $H_2$-TPR experiments, tetrahedral coordinated $WO_x$ species can be assigned as the active sites for the NO reduction by $NH_3$ at high temperatures. In addition, considering that the activity loss with $WO_3$ loading from 25% to 30%, the isolate and dimeric tetrahedral $WO_x$ are much more active than the agglomerated ones.

### 3.2.4. $NH_3$-TPD

Fig. 6 depicts the curves of the $NH_3$-TPD obtained over the W*m*/Ti catalysts. The evolution of ammonia occurs with a broad shape in a wide temperature range, due to the presence of several adsorbed species with different thermal stabilities [28]. In compared with W10/Ti, the peaks of W*m*/Ti ($m \geq 15$) shift to lower temperature (~50 °C), indicating that the $NH_3$ adsorbed species could be more easily desorbed at low temperature with the increasing of $WO_x$.

Surface acidity is considered as a critical role in the SCR reaction in the middle temperature range [29,30]. For W30/Ti sample, the intensity and the area of $NH_3$ desorption peak are comparatively higher than those of other samples because of more acidity sites. This would be the reason of its favorable catalytic activity bellow 400 °C. However, its activity decreases rapidly when the temperature is beyond 400 °C. It indicates that, at high temperatures, the contribution of acidity on the SCR performance can be greatly decreased with the temperature increasing, which are agree well with our activity tests in Fig. 1.

Based on the above experimental results and analyses, for the $WO_3/TiO_2$ catalysts prepared by the sol–gel method, the optimizing loading content of $WO_3$ can be demonstrated as about 25 wt.%. This is not accorded with the results from the samples prepared via the impregnation [11] and co-precipitation method [15]. In addition, the tetrahedral $WO_x$ species have a positive effect on the SCR reaction with the $WO_3$ loading up to 25 wt.%. However, the negative impact appears when the $WO_3$ loading exceeds 25 wt.% because of the tetrahedral species appearing aggregations. The effect of acidity on the SCR performance greatly decreases with the temperature increasing

## 4. Conclusions

In conclusion, $WO_3/TiO_2$ catalysts with different $WO_3$ loading contents have been successfully synthesized via the sol–gel method and their catalytic properties for SCR of NO reduction by $NH_3$ at high temperatures were also investigated. In these samples, the $WO_3$ species were completely dispersed into titania matrix, and the crystalline $WO_3$ phase was undetected with the XRD and Raman spectra even the $WO_3$ loading as high as 30 wt.%. Our experiments have proved that optimizing the addition of tungsten oxide into titania can not only inhibit the size growth of anatase phase but also increase their surface area. Based on the results of the activity test, $H_2$-TPR and $NH_3$-TPD, the sample with 25 wt.% $WO_3$ loading content displays the best catalytic properties. Obviously, the tetrahedral $WO_x$ species as the active site for the $NH_3$-SCR reaction at high temperatures can contribute to the high SCR catalytic performances. And the isolate and dimeric tetrahedral $WO_x$ are much more active than the agglomerated ones. The contribution of acidity on the SCR performance decreases with the temperature increasing.

## Acknowledgments

The authors gratefully acknowledge the financial support from the Scientific and Technological Planning Project of Jilin Province (Grant nos. 20086001 and 20106006), the National 863 Program of China (Grant no. 2007AA06Z316), and China Postdoctoral Science Foundation (Grant no. 20100481063), Zhejiang Provincial Science

Foundation (Grant no. Y4110529), Ningbo Municipal Natural Science Foundation (Grant nos. 2011A610093 and 2011A610094), and China Postdoctoral Science Foundation (Grant no. 20100481063).

## References

[1] H. Bosch, F. Janssen, Catal. Today 2 (1988) 369–379.
[2] M. Koebel, M. Elsener, M. Kleemann, Catal. Today 59 (2000) 335–345.
[3] P. Forzatti, Catal. Today 62 (2000) 51–65.
[4] G. Busca, L. Lietti, G. Ramis, F. Berti, Appl. Catal. B 18 (1998) 1–36.
[5] J.A. Dumesic, N.Y. Topsøe, H. Topsøe, Y. Chen, T. Slabiak, J. Catal. 163 (1996) 409–417.
[6] A.A. Shubin, O.B. Lapina, D. Courcot, Catal. Today 56 (2000) 379–387.
[7] W.Q. Xu, Y.B. Yu, C.B. Zhang, H. He, Catal. Commun. 9 (2008) 1453–1457.
[8] L. Chen, J.H. Li, M.F. Ge, J. Phys. Chem. C 113 (2009) 21177–21184.
[9] L. Chen, J.H. Li, M.F. Ge, R.H. Zhu, Catal. Today 153 (2010) 77–83.
[10] L. Chen, J.H. Li, M.F. Ge, Environ. Sci. Technol. 44 (2010) 9590–9596.
[11] M. Imanari, Y. Watanabe, Stud. Surf. Sci. Catal. 7 (1981) 841–852.
[12] G. Ramis, G. Busca, C. Cristiani, L. Lietti, P. Forzatti, F. Bregani, Langmuir 8 (1992) 1744–1749.
[13] J. Engweiler, J. Harf, A. Baiker, J. Catal. 159 (1996) 259–269.
[14] L. Lietti, J. Svachula, P. Frorzatti, G. Busca, G. Ramis, F. Bregani, Catal. Today 17 (1993) 131–140.
[15] M. Kobayashi, K. Miyoshi, Appl. Catal. B 72 (2007) 253–261.
[16] H.M. Yang, R.R. Shi, K. Zhang, Y.H. Hu, A.D. Tang, X.W. Li, J. Alloys Compd. 398 (2005) 200–202.
[17] Z.F. Zhu, X.M. He, Y. Zhao, Q. Ren, Rare Metal Mater. Eng. 39 (2010) 0771–0774.
[18] M.F. Daniel, B. Desbat, J. Lassegues, B. Gerand, M. Figlarz, Solid State Chem. 67 (1987) 235–240.
[19] M.A. Vurrman, I.E. Wachs, A.M. Hirt, J. Phys. Chem. 95 (1991) 9929–9937.
[20] J.A. Horsley, I.E. Wachs, J.M. Brown, G.H. Via, F.D. Hardcastle, J. Phys. Chem. 91 (1987) 4014–4020.
[21] G. Deo, I.E. Wachs, J. Phys. Chem. 95 (1991) 5889–5895.
[22] A. Schloz, B. Schnyder, A. Wokaun, J. Mol. Catal. A 138 (1999) 249–261.
[23] F.D. Hardcastle, I.E. Wachs, J. Mol. Catal. 46 (1988) 173–186.
[24] S.S. Chan, I.E. Wachs, L.L. Mruuell, J. Catal. 90 (1984) 150–155.
[25] I.E. Wachs, C.C. Chersich, J.H. Hardenberg, Appl. Catal. 13 (1985) 335–346.
[26] D.C. Vermaire, P.C. van Berge, J. Catal. 116 (1989) 309–317.
[27] V.M. Benitez, N.S. Fígoli, Catal. Commun. 3 (2002) 487–492.
[28] L. Lietti, J.L. Alemany, P. Forzatti, G. Busca, G. Ramis, E. Giamello, F. Bregani, Catal. Today 29 (1996) 143–148.
[29] J.P. Chen, R.T. Yang, Appl. Catal. A 80 (1992) 135–148.
[30] L. Lietti, I. Nova, G. Ramis, L. DallAcqua, G. Busca, E. Giamello, P. Forzatti, F. Bregani, J. Catal. 187 (1999) 419–435.